Nanosized Monolayer on Square Lattice within Spin-1 Ising Model: Hysteretic Properties with Odd Interactions

S. Özüm[a,*], R. Kavlak[b], R. Erdem[c] and O. Yalçın[d]

[a] *Alaca Avni Çelik Vocational School, Hitit University, 19600, Çorum, Turkey*
[b] *Institute of Science, Hitit University, 19600 Çorum, Turkey*
[c] *Department of Physics, Akdeniz University, 07058, Antalya, Turkey*
[d] *Department of Physics, Niğde Ömer Halisdemir University, 51240, Niğde, Turkey*

Received: 24.03.2021 & Accepted: 05.05.2021

Doi: 10.12693/APhysPolA.140.84 *e-mail: songulozum@hitit.edu.tr

The hysteretic properties of a nanosized monolayer on the square lattice have been studied based on the spin-1 Ising model, including a single-ion anisotropy (D) and dipolar–quadrupolar (or odd, L) interaction parameters using the pair approximation. The nanosized monolayer is divided into the core, core–surface, and surface parts as introduced in *J. Magn. Magn. Mater.* **373**, 217 (2015). The dipolar (or magnetization M) and quadrupolar (Q) order parameters are calculated. We have investigated M vs. magnetic field H behaviors for different values of L, temperatures T, and monolayer sizes R. We also observed Q–D, M–D and Q–H hysteresis loops. These results are discussed in relation to other theoretical findings.

topics: nanosized monolayer, pair approximation, single-ion anisotropy, odd interaction

1. Introduction

Nanosized monolayer (NML) systems are very important in technology such as capacitive energy storage [1], biomedical applications [2, 3], chemical solution deposition [4], supercapacitors [5], electrocatalytic activity [6, 7], biological cell separation and gold recovery [8]. They have been considered in many theoretical studies where different types of lattice structures were constructed, such as hexagonal lattice, square lattice, nano-graphyne structure, etc. The magnetic and thermal properties of the NML systems on the mentioned lattices, particularly magnetic hysteresis phenomenology, have been analyzed with the use of a variety of techniques, i.e., pair approximation [9–15], effective field theory [16, 17], Monte Carlo simulation [18–22], density functional theory (DFT) [23], finite cluster approximation [24], micromagnetic simulations of switching processes [25, 26] and Lennard-Jones potentials [27]. In most of these studies, the Ising model framework has opened a new path in the research of magnetic/hysteretic properties with different shapes. Particularly, the spin-1 Ising model and its variants on the hexagonal/square lattice NML have attracted much interest [10–17, 20–24].

On the other hand, the spin-1 Ising model with bilinear (J) and biquadratic (K) nearest-neighbor pair interactions and a single-ion anisotropy parameter (D) is known as the Blume–Emery–Griffiths (BEG) model. Firstly, it has been introduced for describing phase separation and superfluid ordering in the He^3–He^4 mixtures [28]. Then, the multiple versions of the model have been applied to the physical systems, such as the spin-1 lattice–gas systems [29], microemulsions [30], semiconductor alloys [31], binary alloy models [32], and spin-crossover solids [33].

The case of the BEG model was studied with different techniques to obtain a complete description of phase transitions arising in bulk systems [34–43]. The model is also exposed by many simulation and approximate techniques to observe various phase regions for the nanostructured lattice types. The Hamiltonian with J, K and D parameters works well in the presence of an external magnetic field (H) for the two-dimensional nanostructures characterized with fluctuations in both magnetic and quadrupolar ordering [11–15]. However, in the case of square lattice NML, the Hamiltonian with the dipolar–quadrupolar or odd interaction (L) has not been considered for the analysis of magnetic and quadrupolar ordering properties [13]. With incorporation of the odd interaction term, the pair approximation (PA) formalism [44] could provide a theoretical framework for the hysteresis loops observed in experiments made on a square lattice NML.

The aim of the present paper is to investigate the effect of L on the hysteretic properties of a spin-1 Ising NML decorated on the square lattice. Within the PA choice, this effect has already been studied successfully for the spin-1 Ising nanoparticle on the hexagonal lattice [14]. Shifted magnetic hysteresis loops with an asymmetry and coercivity enhancement were observed only in the presence of the odd interaction term in the Hamiltonian expression and their magnitudes show strong dependence on the value of L. Hence, the effect of L on the quadrupolar hysteresis has not been taken into account while only the effect on the magnetic hysteresis was analyzed in [14].

In this paper, we would like to present the hysteresis of both magnetization (M) and quadrupole ordering (Q) for the spin-1 Ising NML on the square lattice. Particularly, we analyse in detail the temperature/layer size aspects of the M–H and Q–D dependencies when $L \neq 0$ for homogeneous/composite NML. Also, we obtain the M vs. D and Q vs. H dependence, including novel hysteresis loop shapes for the homogeneous NML.

This paper includes in Sect. 2 a short description of the model and methodology. In Sect. 3, we give the numerical results and discussions. Finally, conclusions have been presented in Sect. 4.

2. Description of model and methodology

A schematic representation of an NML system on the square lattice with two shells is shown in Fig. 1. The filled circles in red and blue colors correspond to the core (C), and surface (S) spins, respectively. They contain core spin number (N_C), core–surface (CS) spin number (N_{CS}) and surface spin number (N_S). The total number of spins in the system is $N = N_C + N_S$. The number of shells inside the layer is related to the size of the system (R). The Hamiltonian for the above spin system can be expressed (in the presence of an external magnetic field H) by [14, 29, 35]:

$$\hat{H} = -J\sum_{\langle ij\rangle} S_iS_j - K\sum_{\langle i,j\rangle} S_i^2S_j^2 - L\sum_{\langle i,j\rangle}\left(S_i^2S_j + S_iS_j^2\right) - D\sum_{\langle i,j\rangle}\left(S_i^2 + S_j^2\right) - H\sum_{\langle i,j\rangle}\left(S_i + S_j\right), \quad (1)$$

where J, K, and L are the dipolar, quadrupolar, and dipolar–quadrupolar exchange energies between the nearest-neighbor atoms (denoted by $\langle ij\rangle$) with spins $S_i = +1, 0, -1$, respectively, while D is the single-ion anisotropy constant (or crystal-field parameter). In (1), the terms with the exchange parameters J and K are even sector contributions, while the magnetic field-like perturbations (L and H) are odd sector terms [34]. Since the parameter L is associated with dipolar and quadrupolar pair interactions, it is combined with J and K via a geometric mean. Namely, $L = \sqrt{JK}$ [45]. All exchange coupling parameters appearing in (1) are given in units of k_BT (where k_B — the Boltzmann constant, T — the temperature). The cases when J, $K > 0$ and when J, $K < 0$ correspond to the ferromagnetic (FM), and the antiferromagnetic (AFM) interactions, respectively. A paramagnetic (PM) phase exists in the system for all temperatures when $J = K = 0$. The fractions of the spin states $(\pm 1, 0)$ are called the point (or state) variables (p_i). In the PA method developed by Kikuchi [44], another sort of variables is introduced, known as bond (or pair) variables (P_{ij}). If the total number of spin pairs in the system is N_p, the number of $(+1,+1)$ bonds is $P_{++}N_p$, of $(+1,0)$ bonds is $P_{+0}N_p$ ($P_{+0} = P_{0+}$), of $(+1,-1)$ bonds is $P_{+-}N_p$ ($P_{+-} = P_{-+}$), the number of $(0,0)$ bonds is $P_{00}N_p$, of $(0,-1)$ bonds is $P_{0-}N_p$ ($P_{0-} = P_{-0}$) and the number of $(-1,-1)$ bonds is $P_{--}N_p$. The relations between point and bond variables are given by $p_i = \sum_{j=+,0,-} P_{ij}$ $(i = +, 0, -)$.

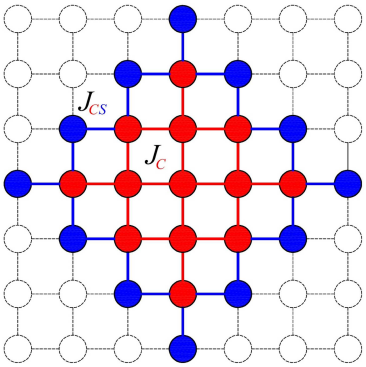

Fig. 1. Schematic representation of a nanosized monolayer on the square lattice exhibiting two shells of the spins. Solid red and blue lines correspond to the core and core–surface pairs, respectively.

We now separate (1) into three terms $(\hat{H}_C, \hat{H}_{CS}, \hat{H}_S)$, including all interactions between the nearest neighboring spins in core (J_C, K_C, L_C, D_C), core–surface (J_{CS}, K_{CS}, L_{CS}), and surface (J_S, K_S, L_S, D_S) regions. Here, $L_C = \sqrt{J_CK_C}$, $L_{CS} = \sqrt{J_{CS}K_{CS}}$, $L_S = \sqrt{J_SK_S}$. Explicit details of the above formulation are presented by Erdem and co-workers for a nanoscale monolayer on the hexagonal lattice in [14, 15]. The dipolar and quadrupolar order parameters are calculated, respectively [15, 41, 46]:

$$M = P_{++} + P_{+0} + P_{+-} - (P_{-+} + P_{-0} + P_{--}), \quad (2)$$

$$Q = P_{++} + P_{+0} + P_{+-} + P_{-+} + P_{-0} + P_{--}. \quad (3)$$

The bond variables are found from the numerical solutions of the following set of equations for $i, j = \{+, 0, -\}$,

$$P_{ij} = Z^{-1}(p_ip_j)^{\frac{\gamma-1}{\gamma}} \exp\left(-\beta\varepsilon_{ij}\right) \equiv Z^{-1}\mathrm{e}_{ij}, \quad (4)$$

TABLE I

Bond energies of spin pairs (i, j) for C, CS, S ions.

	C	CS	S
ε_{++}	$-(J_C + K_C + 2L_C + 2D_C + 2H)$	$-(J_{CS} + K_{CS} + 2L_{CS})$	$-J_S - K_S - 2L_S - 2D_S - 2H$
ε_{+0}	$-(D_C + H)$	0	$-(D_S + H)$
ε_{+-}	$J_C - K_C - 2D_C$	$J_{CS} - K_{CS}$	$J_S - K_S - 2D_S$
ε_{0+}	$-(D_C + H)$	0	$-(D_S + H)$
ε_{00}	0	0	0
ε_{0-}	$-D_C + H$	0	$-D_S + H$
ε_{-+}	$J_C - K_C - 2D_C$	$J_{CS} - K_{CS}$	$J_S - K_S - 2D_S$
ε_{-0}	$-D_C + H$	0	$-D_S + H$
ε_{--}	$-(J_C + K_C - 2L_C + 2D_C - 2H)$	$-(J_{CS} + K_{CS} - 2L_{CS})$	$-(J_S + K_S - 2L_S + 2D_S - 2H)$

where $\beta = 1/(k_B T)$, γ is the coordination number of a given lattice site inside the NML system. The partition function Z is defined with the relation $Z = \sum_{i,j=+,0,-} e_{ij}$. For the energy parameters ε_{ij} in (4) one can introduce the following definition:

$$\varepsilon_{ij} = N_{p,C}\varepsilon_{ij,C} + N_{p,CS}\varepsilon_{ij,CS} + N_{p,S}\varepsilon_{ij,S}, \quad (5)$$

where $N_{p,C} = \frac{1}{2}N_C\gamma_C - N_{CS}$, $N_{p,CS} = N_{CS}\gamma_{CS}$, $N_{p,S} = \frac{1}{2}N_S\gamma_S$ are the numbers of spin pairs (with $\gamma_C = 4$, $\gamma_{CS} = 2$, $\gamma_S = 0$) and $\varepsilon_{ij,C}$, $\varepsilon_{ij,CS}$, $\varepsilon_{ij,S}$ are called the bond energies of spin pairs (ij) for C, CS, S ions, respectively [11–15]. Their computed values, by using (1), are presented in Table I. To solve the nonlinear algebraic equations (4), the Newton–Raphson or iteration method was applied. After establishing the P_{ij} values, M and Q can be obtained easily using, respectively, (2) and (3).

In the next section, we examine the hysteretic properties of M and Q at various temperatures, magnetic fields, and layer sizes under $L \neq 0$.

3. Results and discussion

In the numerical calculations presented below, we focus on two different cases, which will let us study the effect of interactions across the CS interface on the hysteresis phenomena. The monolayer with the FM core / FM core–surface interactions with $J_C = J_{CS} = J = 1$, $K_C = K_{CS} = K$ is called the homogeneous (HM) NML. In turn, the FM core / AFM core–surface interactions with $J_C = J = 1$, $J_{CS} = -J$, $K_C = K$, $K_{CS} = -K$ is known as the composite (CM) NML. For simplicity, we chose $L_C = L_{CS} = L$ and $D_C = D$ in both cases. As for the bilinear, biquadratic, and odd interactions between surface spins (J_S, K_S,L_S) we did not consider contribution to total magnetization. Quadrupole moment appeared from the surface part because of zero lattice coordination ($\gamma_S = 0$), as shown in Fig. 1.

The magnetization M as a function of H and the quadrupolar order parameter Q as a function of D for the HM- and CM-NML with six shells of spins are performed at $T = 100\ J/k_B$ and the results are displayed in Fig. 2. Taking $D = -1$, three hysteresis curves are shown for the HM-NML

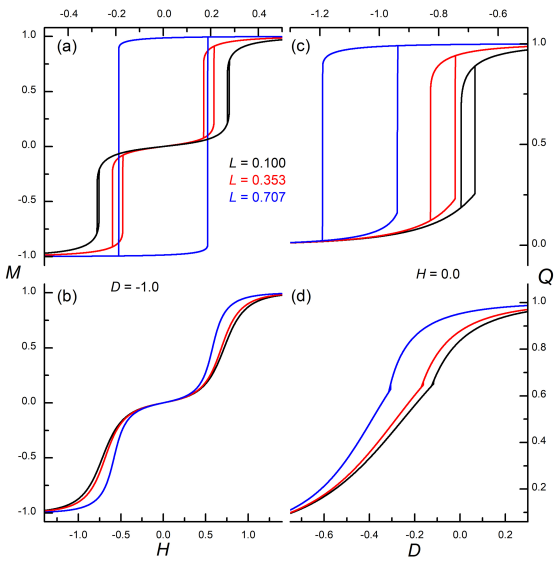

Fig. 2. Magnetic field H dependence of M when $D = -1$ and crystal field D dependence of Q when $H = 0$ at various L values using $R = 6$, $T = 100\ J/k_B$. The cases (a) and (c) are for the HM-NML while (b) and (d) for the CM-NML.

(see Fig. 2a). As indicated, the hysteresis loop is regular and symmetrical around $H = 0.0$ when $L = 0.707$ (blue curve), while double FM loops are observed at $L = 0.100$ (black curve) and $L = 0.353$ (red curve). When L increases, the split loops become wider. The isothermal magnetic field dependence of M at $D = -1$ shows the PM-type behavior for all L values (see Fig. 2b), as for the CM-NML. The single M–H line is based on the same direction pinned spins, at C/S interface. A detailed discussion of the above results can be found in [20]. The quadrupolar order parameter Q in the absence of magnetic field is plotted as a function of D for the interaction parameters used in the previous two cases (a) and (b). According to our calculations (see Fig. 2c and d), the Q vs. D curves also display a loop shape, which is generally called as the quadrupolar hysteresis. As the odd interaction L increases, the single loop becomes wider and shifts along the negative D direction for the HM-NML, as shown in Fig. 2c. Conversely, the shifted Q–D

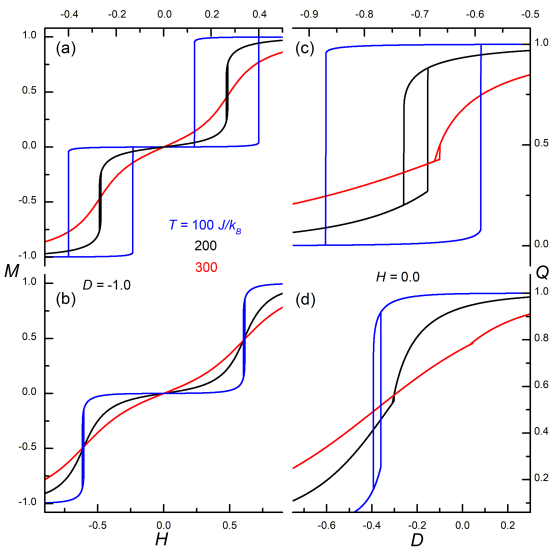

Fig. 3. Description as in Fig. 2 but for different temperatures using $R = 8$, $K = 0.125$, $L = 0.353$.

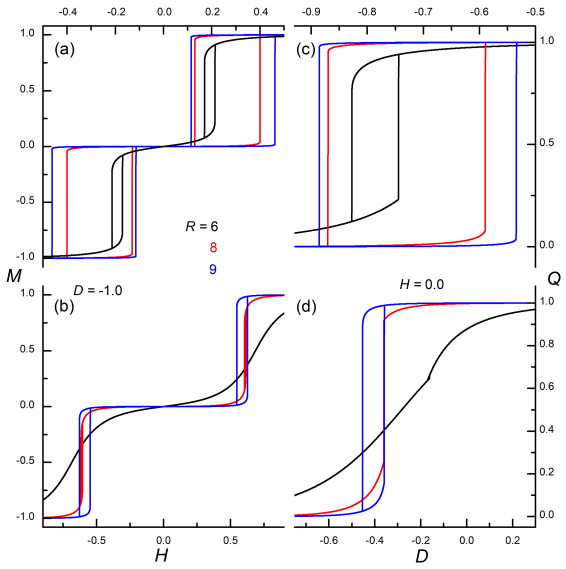

Fig. 4. Description as in Fig. 3 but for different layer sizes using $T = 100\ J/k_{\rm B}$.

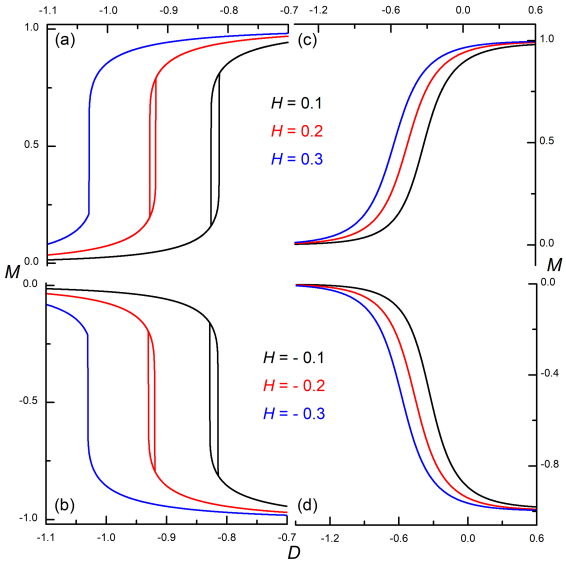

Fig. 5. Crystal field D dependence of M on various magnetic field values using $R = 6$, $T = 100\ J/k_{\rm B}$, $K = 0.01$, $L = 0.1$. The left side is for the HM-NML, while the right side is for the CM-NML.

loops seen for the CM-NML in Fig. 2d are very small. A similar feature reveals as the exchange bias (EB) effect in the magnetic hysteresis phenomena and is determined from the horizontal shift in the midpoint of the loop [14, 47, 48]. Perhaps one can say that the EB-like effects can also be seen in the Q–D loops. In other words, EB-like results from the coupling between the pinned spins, is strongly influenced by the surface anisotropy and the reversible spins. For a similar analysis of the above loops in the 2D spin-1 Ising nanostructures, please see [15].

In Fig. 3, the M–H and Q–D curves are given at three different temperatures, i.e., $T = 100$, 200, 300 $J/k_{\rm B}$ and assuming $R = 8$, $K = 0.125$, $L = 0.353$. As one can notice, the curves strongly depend on the temperature. For example, the split hysteresis (or double FM loops) become wide for the HM-NML when T decreases and the PM behavior occurs when T increases (see Fig. 3a). Similar results are also presented for the CM-NML in Fig. 3b. We noted there that for increasing values of T from 100 $J/k_{\rm B}$ to 300 $J/k_{\rm B}$, the split loops become narrower and further disappear for the CM-NML. In contrast to the symmetric magnetic hysteresis, an asymmetric loop is observed in Q vs. D variation for the NML.

Asymmetry of the Q–D loops without magnetic field is generally attributed to the permanent magnetic moment and the single ion anisotropy. Moreover, these asymmetric loops become narrow with increasing temperature for the HM- and CM-NML, as can be seen in Fig. 3c and d, respectively. The narrowing loops in the Q–D plane eventually disappear at very high temperatures (see Fig. 3d). Looking at the shapes of the obtained loops (Fig. 3c and d), one can observe that there is a shift towards the positive D direction when the temperature is raised from $T = 100\ J/k_B$ to 300 $J/k_{\rm B}$.

In Fig. 4, we have presented the M–H and Q–D hysteresis cycles of the spin-1 Ising NML on a decorated square lattice for various values of R when $T = 100\ J/k_B$, $K = 0.125$, $L = 0.353$. With the increase of layer sizes R for the HM-NML, double and asymmetric M–H loops occur in Fig. 4b. Double PM shapes are obtained at small R sizes for the CM-NML in Fig. 4b. Asymmetric Q–D hysteresis loops shifting as R increases along the positive and negative D direction are shown in Fig. 4c and d, respectively, and correspond to the HM/CM-NML.

In Fig. 5, we plot the magnetization of the system as a function of the crystal field D for various values of external magnetic field H, for both the

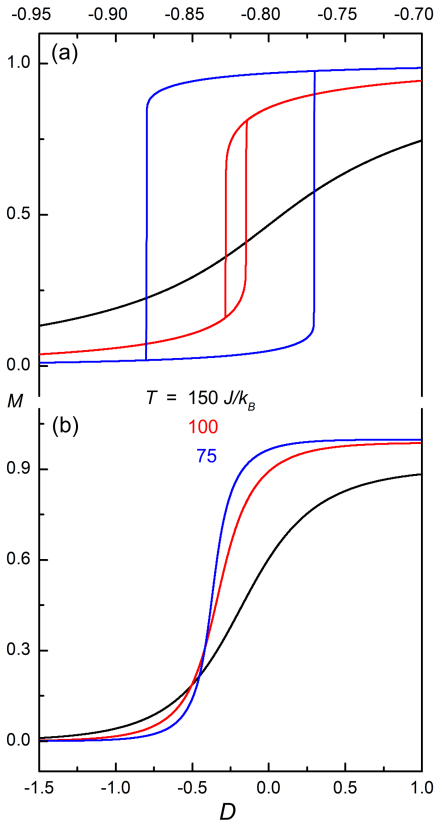

Fig. 6. Magnetization M as a function of D at various temperatures when $R = 6$, $K = 0.01$, $L = 0.1$, $H = 0.1$. (a) is for the HM-NML while (b) is for the CM-NML.

HM- and CM-NML. We take the following values $R = 6$, $T = 100\ J/k_{\rm B}$, $K = 0.01$, $L = 0.1$. In the HM case, M increases (decreases) from diverse values, at $D = -1.1$ with the increase of D, when $H > 0$ ($H < 0$) as shown in Fig. 5a (Fig. 5b), respectively. The saturation values of $M \approx \pm 1.0$ occur at $D \approx -0.65$ when $H = \pm 0.1$, ± 0.2, ± 0.3. A single FM loop, which is seen at intermediate crystal fields, becomes wider with decreasing H value. However, for the CM case (Fig. 5c and d), we observe no hysteresis, and rather a shifted PM curve (towards the negative D direction) appears. We also note that when changing the sign of H, the tendencies are opposite, which comes from the fact that two spins are oppositely aligned. Several of the above results have also been identified in previous theoretical studies [49, 50].

In Fig. 6, we show the M–D behavior at different temperatures for the monolayer systems already described, and choosing $H = 0.1$. It is clear that the FM loops in the HM case become narrower and disappear with increasing temperature (see Fig. 6a). The PM behaviors have been observed for the CM-NML, as seen in Fig. 6b. Also, it is worth noting that all magnetization curves cross at the crystal field $D \approx -0.5$ for all values of the temperature, see Fig. 6b. Hence, we conclude that M increases

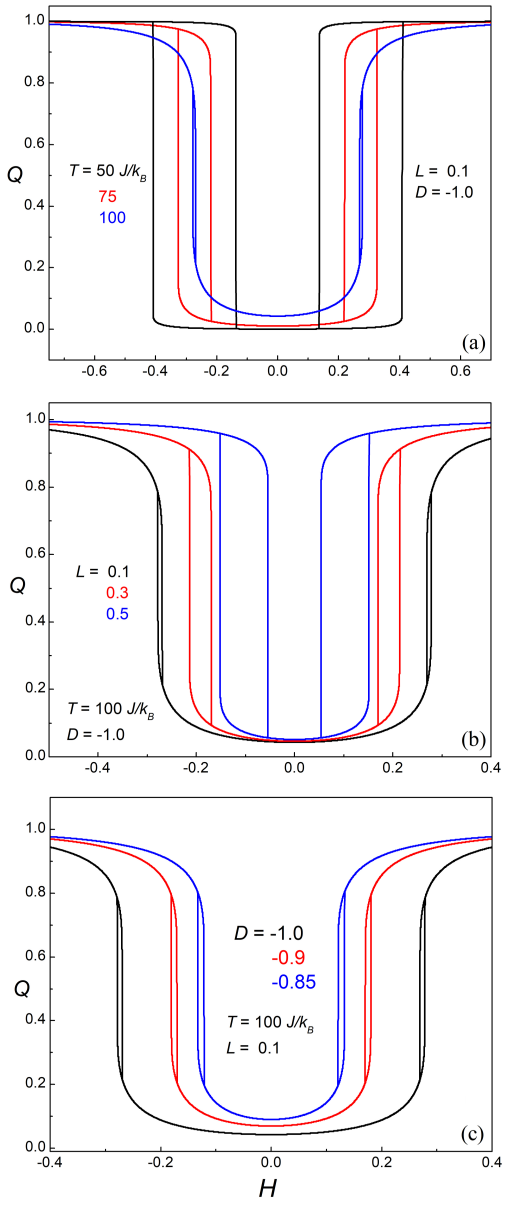

Fig. 7. The Q–H hysteresis loops at various values of (a) T, (b) L, (c) D for the HM-NML with $R = 6$.

rapidly to its saturation value $M \approx 1$ with increasing D, when $H = 0.1$, for small temperatures. A similar picture of variation of magnetization with the crystal field is found in a Blume–Capel model with the mixed 2- and 7/2-spins using the Monte Carlo simulation [49].

Finally, in Fig. 7, the quadrupole moment Q is plotted as a function of the external magnetic field H for various values of T, L, D for the HM-NML with $R = 6$. In this case, two FM loops in the negative and positive direction of H are obtained. Upon increasing the temperature T, both loops become narrower and no shift is seen (Fig. 7a). In turn, the increase of L values causes that wider loops are seen with a shift towards each other (Fig. 7b). In Fig. 7c, two FM loops are observed at different values of D in both directions of H. These loops shift to each

other when D grows. To the best knowledge of the authors, the above closed loops and the corresponding properties in the Q–H behavior for the spin-1 Ising NML systems have not been previously depicted. The aspect of the magnetic field variation of the quadrupole moment was investigated for the one-dimensional spin-1 BEG model using Green's function and the equations of motion formalism focusing on the role played by the biquadratic interaction and crystal field [51, 52].

4. Conclusion

In this paper, we have used the pair approximation technique to examine the hysteretic properties with odd interactions for the nanosized monolayer on the square lattice within the spin-1 Ising model. We have studied the variations of the magnetization and quadrupolar order as functions of the magnetic and crystal fields. This issue was studied under the effects of the odd interaction, monolayer size, temperature and the external magnetic field. The analysis allows for a comprehensive analysis of the model in the entire space of parameters L, D, H, R, and T. The investigation of hysteretic properties of an NML system revealed consistent results with the earlier works on the same topic. Here, we have focused on the ferromagnetism exhibited by the model used. There are remarkable properties of M–H, Q–D, M–D and Q–H that are worth discussing. In particular, upon increasing the value of the odd interaction, one observes the breakdown of the intermediate plateau, resulting in a uniform quadrupolar moment for all values of the magnetic field on Q–H plots. Also, the double FM and PM phases have been detected.

References

[1] Y. Lv, W. Lei, S. Liu, W.-H. Zhang, *Adv. Electron. Mater.* **5**, 1800830 (2019).

[2] R. Bhure, T.-M. Abdel-Fattah, C. Bonner, J.C. Hall, A. Mahapatro, *J. Biomed. Nanotechnol.* **6**, 117 (2010).

[3] S. Rajashekara, A. Shrivastava, S. Sumhitha, S. Kumari, *BioNanoScience* **10**, 654 (2020).

[4] A. Mukherjee, P. Mitra, *Indian J. Phys.* **89**, 1007 (2015).

[5] B. Ankamwar, P. Das, U.K. Sur, *Indian J. Phys.* **90**, 391 (2016).

[6] S. Zhao, S. Chen, S. Wang, S. Lei, Z. Quan, *Thin Solid Films* **360**, 56 (2000).

[7] K.A. Friedrich, F. Henglein, U. Stimming, W. Unkauf, *Electrochim. Acta* **45**, 3283 (2000).

[8] Q. Liu, Z. Xu, *Langmuir* **11**, 4617 (1995).

[9] L.G.C. Rego, W. Figueiredo, *Phys. Rev. B* **64**, 144424 (2001).

[10] O. Yalçın, R. Erdem, S. Övünç, *Acta Phys. Pol. A* **114**, 835 (2008).

[11] O. Yalçın, R. Erdem, S. Özüm, *J. Appl. Phys.* **115**, 054316 (2014).

[12] O. Yalçın, R. Erdem, S. Özüm, Z. Demir, *J. Magn. Magn. Mater.* **389**, 120 (2015).

[13] S. Özüm, O. Yalçın, R. Erdem, H. Bayrakdar, H.N. Eker, *J. Magn. Magn. Mater.* **373**, 217 (2015).

[14] R. Erdem, O. Yalçın, S. Özüm, N. Çiftçi, *Adv. Condens. Matter Phys.* **2016**, 6563274 (2016).

[15] R. Erdem, O. Yalçın, S. Özüm, A. Şahin, N. Demirer, *Chin. J. Phys.* **69**, 38 (2021).

[16] E. Kantar, M. Keskin, *J. Magn. Magn. Mater.* **349**, 165 (2014).

[17] S. Bouhou, M. El Hamri, I. Essaoudi, A. Ainane, R. Ahuja, F. Dujardin, *Chin. J. Phys.* **55**, 2224 (2017).

[18] E.V. Albano, K. Binder, D.W. Heermann, W. Paul, *Z. Phys. B Condens. Matter* **77**, 445 (1989).

[19] A.J. Ramirez-Pastor, J.L. Riccardo, V.D. Pereyra, *Surf. Sci.* **411**, 294 (1998).

[20] S. Aouini, S. Ziti, H. Labrim, L. Bahmad, *J. Supercond. Nov. Magn.* **30**, 455 (2017).

[21] A. Jabar, R. Masrour, *Physica A* **515**, 270 (2019).

[22] Z. Fadil, A. Mhirech, B. Kabouchi, L. Bahmad, W.O. Benomar, *Superlatt. Microstruct.* **135**, 106285 (2019).

[23] N. Wang, Y. Tian, J. Zhao, P. Jin, *J. Mol. Graph. Model.* **66**, 196 (2016).

[24] M. Mouhib, N. Benayad, M. Azhari, *J. Magn. Magn. Mater.* **419**, 325 (2016).

[25] L. Torres, E. Martinez, L. Lopez-Diaz, J. Iñiguez, *J. Appl. Phys.* **89**, 7585 (2001).

[26] M. Maicas, M. Rodríguez, E. López, M.C. Sánchez, C. Aroca, P. Sánchez, *Comput. Mater. Sci.* **25**, 525 (2002).

[27] O. Biham, L.-W. Chen, G. Vidali, *Surf. Sci.* **287/288**, 815 (1993).

[28] M. Blume, V.J. Emery, R.B. Griffiths, *Phys. Rev. A* **4**, 1071 (1971).

[29] J. Sivardière, J. Lajzerowicz, *Phys. Rev. A* **11**, 2090 (1975).

[30] M. Schick, W.H. Shih, *Phys. Rev. B* **34**, 1797 (1986).

[31] B.L. Gu, J. Ni, J.L. Zhu, *Phys. Rev. B* **45**, 4071 (1992).

[32] M. Kessler, W. Dieterich, A. Majhofer, *Phys. Rev. B* **67**, 134201 (2003).

[33] T.D. Oke, F. Hontinfinde, K. Boukheddaden, *Eur. Phys. J. B* **86**, 271 (2013).

[34] A.N. Berker, M. Wortis, *Phys. Rev. B Condens. Matter* **14**, 4946 (1976).

[35] Y. Saito, *J. Chem. Phys.* **74**, 713 (1981).

[36] W. Hoston, A.N. Berker, *Phys. Rev. Lett.* **67**, 1027 (1991).

[37] A. Rosengren, S. Lapinskas, *Phys. Rev. B* **47**, 2643 (1993).

[38] M. Keskin, C. Ekiz, O. Yalçın, *Physica A* **267**, 392 (1999).

[39] M. Gzik-Szumiata, T. Balcerzak, *Acta Phys. Pol. A* **97**, 939 (2000).

[40] R. Erdem, C. Ekiz, M. Keskin, *Phys. Status Solidi B* **240**, 220 (2003).

[41] M. Keskin, A. Erdinç, *J. Magn. Magn. Mater.* **283**, 392 (2004).

[42] H.P. Dong, S.L. Yan, *J. Magn. Magn. Mater.* **308**, 90 (2007).

[43] M. Keskin, B. Deviren, O. Canko, M. Kirak, *Acta Phys. Pol. B* **38**, 2445 (2007).

[44] R. Kikuchi, *J. Chem. Phys.* **60**, 1071 (1974).

[45] C. Temirci, A. Kökçe, M. Keskin, *Physica A* **231**, 673 (1996) and references therein.

[46] A. Erdinç, M. Keskin, *Physica A* **307**, 453 (2002).

[47] U. Wiedwald, J. Lindner, M. Spasova, Z. Frait, M. Farle, *Phase Transit.* **78**, 85 (2005).

[48] X.H. Huang, J.F. Ding, G.Q. Zhang, Y. Hou, Y.P. Yao, X.G. Li, *Phys. Rev. B* **78**, 224408 (2008).

[49] R. Masrour, A. Jabar, L. Bahmad, M. Hamedoun, A. Benyoussef, *J. Magn. Magn. Mater.* **421**, 76 (2017).

[50] H. Bouda, T. Bahlagui, L. Bahmad, R. Masrour, A. El Kenz, A. Benyoussef, *J. Supercond. Nov. Magn.* **32**, 2539 (2019).

[51] F.P. Mancini, *J. Phys. Conf. Series* **200**, 022030 (2010).

[52] F. Mancini, F.P. Mancini, *Condens. Matter Phys.* **11**, 543 (2008).